# Disorder-promoted C_{4}-symmetric magnetic order in iron-based superconductors

Mareike Hoyer, Rafael M. Fernandes, Alex Levchenko, and Jörg Schmalian

Phys. Rev. B **93**, 144414 — Published 18 April 2016

DOI: 10.1103/PhysRevB.93.144414

# Disorder-promoted $C_4$-symmetric magnetic order in iron-based superconductors

Mareike Hoyer,[1,2] Rafael M. Fernandes,[3] Alex Levchenko,[4] and Jörg Schmalian[1,2]

[1] *Institut für Theorie der Kondensierten Materie, Karlsruher Institut für Technologie, D-76131 Karlsruhe, Germany*

[2] *Institut für Festkörperphysik, Karlsruher Institut für Technologie, D-76021 Karlsruhe, Germany*

[3] *School of Physics and Astronomy, University of Minnesota, Minneapolis 55455, USA*

[4] *Department of Physics, University of Wisconsin-Madison, Madison, Wisconsin 53706, USA*

(Dated: March 30, 2016)

In most iron-based superconductors, the transition to the magnetically ordered state is closely linked to a lowering of structural symmetry from tetragonal ($C_4$) to orthorhombic ($C_2$). However, recently, a regime of $C_4$-symmetric magnetic order has been reported in certain hole-doped iron-based superconductors. This novel magnetic ground state can be understood as a double-$\mathbf{Q}$ spin density wave characterized by two order parameters $\mathbf{M}_1$ and $\mathbf{M}_2$ related to each of the two $\mathbf{Q}$ vectors. Depending on the relative orientations of the order parameters, either a noncollinear spin-vortex crystal or a nonuniform charge-spin density wave could form. Experimentally, Mössbauer spectroscopy, neutron scattering, and muon spin rotation established the latter as the magnetic configuration of some of these optimally hole-doped iron-based superconductors. Theoretically, low-energy itinerant models do support a transition from single-$\mathbf{Q}$ to double-$\mathbf{Q}$ magnetic order, but with nearly-degenerate spin-vortex crystal and charge-spin density wave states. In fact, extensions of these low-energy models including additional electronic interactions tip the balance in favor of the spin-vortex crystal, in apparent contradiction with the recent experimental findings. In this paper, we revisit the phase diagram of magnetic ground states of low-energy multi-band models in the presence of weak disorder. We show that impurity scattering not only promotes the transition from $C_2$ to $C_4$-magnetic order, but it also favors the charge-spin density wave over the spin-vortex crystal phase. Additionally, in the single-$\mathbf{Q}$ phase, our analysis of the nematic coupling constant in the presence of disorder supports the experimental finding that the splitting between the structural and stripe-magnetic transition is enhanced by disorder.

## I. INTRODUCTION

One of the common features of iron-based superconductors (FeSC) is the emergence of superconductivity in close proximity to a magnetic instability.[1,2] Even more intriguingly, superconductivity coexists with magnetism in some of the iron-based compounds.[3,4] Thus it is imperative to study the nature of the magnetic order in the FeSC compounds in order to better understand the superconducting state in these materials.

Most of the undoped compounds of the FeSC family exhibit magnetic stripe order with the spins on the iron sites lying in the planes and being aligned ferromagnetically along one direction, and antiferromagnetically along the other. In addition to the continuous $O(3)$ spin-rotational symmetry broken below the magnetic transition temperature $T_{\rm N}$, this stripe-magnetic (SM) state also breaks an additional $\mathbb{Z}_2$ Ising-like symmetry since the ordering vector of the spin density wave (SDW) $\mathbf{S}(\mathbf{r}) = \mathbf{M}e^{i\mathbf{Q}\cdot\mathbf{r}}$ is either $\mathbf{Q} = (0,\pi)$ or $\mathbf{Q} = (\pi,0)$. This $\mathbb{Z}_2$ (or, equivalently, $C_2$) symmetry breaking can occur at temperatures $T_{\rm s} > T_{\rm N}$ and entails a structural transition from tetragonal ($C_4$) to orthorhombic ($C_2$). Furthermore, if the transitions are split, this allows for an intermediate phase with broken $\mathbb{Z}_2$ symmetry but no magnetic long-range order. This intermediate phase is dubbed *nematic order*[5–7]. Interestingly, the splitting $\Delta T = T_{\rm s} - T_{\rm N}$ between the two transitions, and the stabilization of an intermediate nematic phase, depends on disorder.[8–10]. Uncovering the origin of the nematic phase – either a spin-driven or an orbital-driven mechanism – may also elucidate the mechanism for superconductivity.

Recently, $C_4$-magnetic phases have been observed in the hole-doped compounds $Ba(Fe_{1-x}Mn_x)_2As_2$,[11] $Ba_{1-x}Na_xFe_2As_2$,[12,13], $Ba_{1-x}K_xFe_2As_2$,[14–17] and $Sr_{1-x}K_xFe_2As_2$[18], suggesting that such phases might be a general feature in the phase diagram of hole-doped FeSC[19]. The magnetic Bragg peaks of these $C_4$-magnetic phases occur at the same momenta $\mathbf{Q}_1 = (\pi,0)$ and $\mathbf{Q}_2 = (0,\pi)$ as in the stripe-ordered state and, consequently, such a state can be understood as the superposition of two spin density waves $\mathbf{S}(\mathbf{r}) = \mathbf{M}_1 e^{i\mathbf{Q}_1\cdot\mathbf{r}} + \mathbf{M}_2 e^{i\mathbf{Q}_2\cdot\mathbf{r}}$, i. e. a double-$\mathbf{Q}$ SDW, as illustrated in Fig. 1. As in the case of stripe antiferromagnetism, which is preceded by nematic order, these double-$\mathbf{Q}$ magnetic states can in principle be melted in two stages as well, passing through an intermediate state of vestigial charge or chiral order.[20]

The existence of double-$\mathbf{Q}$ magnetic states as additional ground states for the FeSC has also been established by different theoretical approaches,[21–29] all of which suggest the two possible double-$\mathbf{Q}$ ground states visualized in Fig. 1 in addition to the single-$\mathbf{Q}$ stripe-magnetic order. Fig. 1(a) shows the *charge-spin density wave* (CSDW) that arises from aligning $\mathbf{M}_1$ and $\mathbf{M}_2$ either parallel or antiparallel. This results in a nonuniform magnetization with vanishing average moment at the even lattice sites and staggered-like order at the odd lattice sites, or vice versa. This magnetic state is ac-

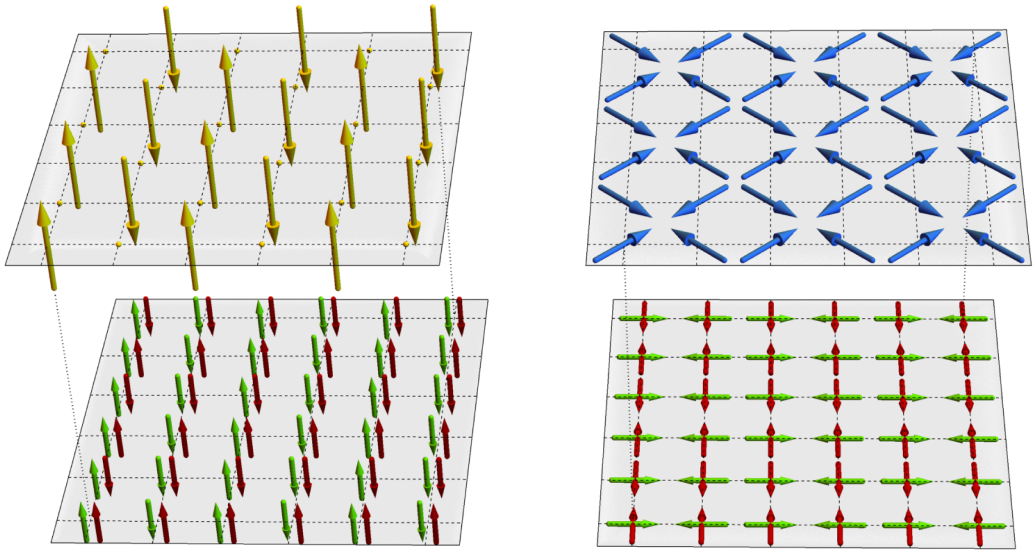

(a) charge-spin density wave (b) spin-vortex crystal

FIG. 1. Illustration of the two double-**Q** magnetically ordered states (upper panels) as a superposition of two single-**Q** stripe-magnetic states (lower panels). (a) Aligning the order parameters $\mathbf{M}_1 = \pm\mathbf{M}_2$ (anti)parallel yields a charge-spin density wave. This order is favorable if $g < |w|$ and $w < 0$. (b) Aligning the order parameters $\mathbf{M}_1 \perp \mathbf{M}_2$ perpendicular to each other leads to the formation of a spin-vortex crystal. This state is favorable if $g < 0$ and $w > 0$. Otherwise, single-**Q** stripe order is favored.

companied by charge density wave order since it couples naturally to a modulation of the density:[20] The charge couples to the square of the magnetization, thus the magnetic sites acquire a charge that is different from the nonmagnetic sites. If $\mathbf{M}_1$ and $\mathbf{M}_2$ are orthogonal, the resulting *spin-vortex crystal* (SVC) is characterized by a noncollinear magnetization that is illustrated in Fig. 1(b).

All three magnetic states, the stripe-magnetic and the two double-**Q** magnetic states, can be rationalized in terms of a Ginzburg-Landau expansion of the free energy in terms of the two magnetic order parameters $\mathbf{M}_i$[20,26,30],

$$F[\mathbf{M}_i] = a\left(\mathbf{M}_1^2 + \mathbf{M}_2^2\right) + \frac{u}{2}\left(\mathbf{M}_1^2 + \mathbf{M}_2^2\right)^2 - \frac{g}{2}\left(\mathbf{M}_1^2 - \mathbf{M}_2^2\right)^2 + 2w\left(\mathbf{M}_1 \cdot \mathbf{M}_2\right)^2 \quad . \quad (1)$$

Depending on the quartic coefficients $u$, $g$, and $w$, the corresponding energy is minimized by one of the three magnetic ground states described above, provided that $u > \max(0, g, -w)$.

For $g > \max(0, -w)$, the stripe-ordered $C_2$-magnetic phase is the magnetic ground state of systems described by the free energy (1), and it is accompanied by a structural transition from tetragonal to orthorhombic. This scenario is supported by itinerant as well as by localized approaches to magnetism in FeSC, and it is experimentally well established that stripe-SDW is the magnetic ground state of many compounds of this family of materials. If, on the other hand, $g < \max(0, -w)$, one of the two above described possibilities of $C_4$-magnetic phases is realized, depending on whether $w > 0$ (leading to a spin vortex crystal) or $w < 0$ (implying a charge-spin density wave). Note that further away from the magnetic phase transition, higher-order terms that favor the stripe-magnetic state might become relevant. Indeed, the experimentally observed re-entrance of the $C_2$-magnetic phase upon lowering the temperature can be explained in terms of a Ginzburg-Landau expansion of the clean three-band model if sixth-order terms are taken into account.[28]

Experimentally, several probes[18,31,32] established that the magnetic moments in the $C_4$-magnetic phase observed in hole-doped FeSC are aligned parallel to the $c$ axis, i. e. pointing out of plane, and that the magnetic moment vanishes at every second lattice site while it is doubled at the others. These features uniquely identify this $C_4$-magnetic phase as a realization of a charge-spin density wave, corresponding to $w < 0$. Therefore, it is important to elucidate theoretically which generic features of low-energy models yield $w < 0$ and $g < |w|$.

Localized approaches based on the $J_1$-$J_2$ Heisenberg model favor the single-**Q** stripe-ordered state,[33] whereas itinerant approaches allow for both signs of $g$. Focusing on the three-band itinerant low-energy model previously employed in the literature[19,22,26], one finds a sign-change from $g > 0$ near perfect nesting to $g < 0$ away from perfect nesting, implying a transition from single-**Q** to a double-**Q** state. This sign change coincides with a decrease of the magnitude of the coupling constant,[28] indicating that the overall weakening of magnetic order allows for the $C_4$ phase. However, due to phase space restrictions, this same model generically gives $w = 0$ (for details, see Sect. II A), leaving the noncollinear SVC and

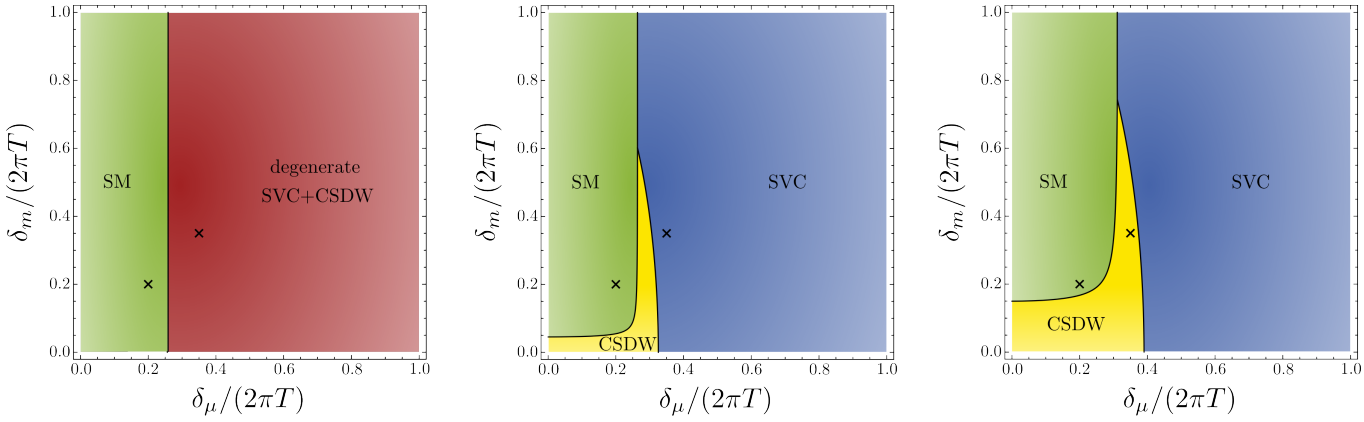


(a) $\frac{\rho_F \Gamma_h^{\text{intra}}}{4T} = 0$ (b) $\frac{\rho_F \Gamma_h^{\text{intra}}}{4T} = 0.01$ (c) $\frac{\rho_F \Gamma_h^{\text{intra}}}{4T} = 0.1$

FIG. 2. Evolution of the phase diagrams of the possible magnetic ground states of our three-band minimal model of iron-based superconductors upon increase of the scattering rate. Here, we used $\Gamma_{e-e}^{\text{inter}} = 0.1\Gamma_h^{\text{intra}}$, and the phase diagrams are obtained in the limit $\delta_\mu \ll 2\pi T$ and $\delta_m \ll 2\pi T$. The regime of single-**Q** stripe order (SM) is shown in green, the double-**Q** spin-vortex crystal (SVC) order is indicated by blue, and the yellow region represents the double-**Q** charge-spin density wave (CSDW). In the clean regime, where all scattering rates are zero, SVC and CSDW order are degenerate and we indicated this region with $w = 0$ in red. The crosses mark the points in the phase diagram at which we plotted $g$ and $w$ as a function of scattering rate in Fig. 5 and Fig. 7, respectively.

the nonuniform CSDW order degenerate [see Fig. 2(a)]. Extensions of this model tend to favor $w > 0$, in disagreement with the recent experiments – this is indeed obtained by including residual electronic interactions[19,22] or, as we will show below, an incipient fourth pocket. We note that although Ref. 30 proposed that the proximity to a Néel-like state can favor $w < 0$, this scenario is only applicable to $Ba(Fe_{1-x}Mn_x)_2As_2$, since the compound $BaMn_2As_2$ displays Néel order – which is not the case for $Ba_{1-x}Na_xFe_2As_2$ or $Ba_{1-x}K_xFe_2As_2$. Note also that Ref. 34 showed that the spin-orbit coupling leads to anisotropic quadratic terms in the free energy (1) that favor the CSDW order, even though $w = 0$. This however only works near the magnetic transition, since at low temperatures the quartic terms are the ones that determine the ground state.

Therefore, understanding which additional features can lead to $w < 0$ is essential to shed light on the mechanisms behind the formation of the $C_4$ phase. Since charged potential impurities can locally stabilize charge-spin density wave order,[21,29] one promising approach is the inclusion of doping effects beyond a rigid-band model. In this paper, we consider the effect of impurity scattering on the quartic coupling constants $g$ and $w$ of the itinerant minimal three-band model. We find that, in the regime where $g > 0$ in the clean system, the inclusion of disorder suppresses $g$, and may even change its sign. One of the consequences of this result is that the splitting $\Delta T = T_s - T_N$ between the structural and magnetic transitions to the stripe-ordered state may, depending on the vicinity of the system to a tricritical point, enhance upon increasing disorder, in agreement with recent experiments on $BaFe_2As_2$ subject to electron irradiation[9]. Furthermore, disorder itself may cause a transition from single-**Q** to double-**Q** order near perfect nesting, as shown in Figs. 2(b) and (c). Our most important result, however, is the fate of the vanishing coefficient $w$ in the presence of disorder. We find that disorder generally lifts the degeneracy between CSDW and SVC, favoring $w < 0$ (and therefore CSDW) near perfect nesting [Figs. 2(b) and (c)]. Consequently, this opens the interesting possibility of controlling the magnetic ground state in FeSC with controlled disorder introduced via irradiation or removed via annealing.

The paper is structured as follows. Section II introduces the microscopic model including disorder, which we use to calculate the free energy. We start by recapitulating that $w = 0$ follows immediately from a three-band model in Section II A, followed by the discussion of a fourth band in Section II B which only allows for $w > 0$. Consequently, we study the effect of disorder as an alternative route and show in Section II C that the presence of impurities can indeed render $w < 0$ already within the simpler three-band model. The nature of the magnetic ground state is determined by the coefficients $g$ and $w$, and their dependence on disorder is discussed in Section III, also elucidating the disorder dependence of the splitting between nematic and magnetic transition. Finally, we combine our results to obtain a phase diagram of magnetic ground states in the presence of disorder, which complements the discussion of our conclusions in Section IV.

## II. MICROSCOPIC MODEL

We consider a minimal multi-band model[22,26] for iron-based superconductors (FeSC), consisting of two circular hole pockets centered around the $\Gamma$ point and the $M$ point of the Fe-only Brillouin zone, i. e. around $(0,0)$ and $(\pi,\pi)$, respectively, and two elliptical electron pockets centered around $X$ and $Y$ at $\mathbf{Q}_1 = (\pi,0)$ and $\mathbf{Q}_2 = (0,\pi)$, respectively. The pocket at the $M$ point however is not a generic feature of this class of materials since it exists only in some of the iron-based compounds. Moreover, even in the compounds in which the pocket at the $M$ point exists, this band is not guaranteed to cross the Fermi level for all values of $k_z$. Our analysis in Section II B will show that the presence of such an incipient hole pocket at the $M$ point cannot explain the formation of a charge-spin density wave and hence can be neglected in the remainder of this paper.

The noninteracting part of the model is described by the Hamiltonian

$$\mathcal{H}_0 = \sum_{\mathbf{k},\sigma,\lambda} \varepsilon_{\lambda,\mathbf{k}} c^\dagger_{\lambda,\mathbf{k},\sigma} c_{\lambda,\mathbf{k},\sigma} \ , \tag{2}$$

where the fact that the bands are centered around different momenta is reflected in the band index $\lambda \in \{\mathrm{h}_1, \mathrm{h}_2, \mathrm{e}_1, \mathrm{e}_2\}$ where the hole bands are labeled by $\mathrm{h}_1 \equiv \mathrm{h}_\Gamma$ and $\mathrm{h}_2 \equiv \mathrm{h}_M$, and the electron bands by $\mathrm{e}_1 \equiv \mathrm{e}_X$ and $\mathrm{e}_2 \equiv \mathrm{e}_Y$. Thus $c^\dagger_{\lambda,\mathbf{k},\sigma}$ creates an electron in band $\lambda$ with spin $\sigma$, and the respective dispersions near the Fermi energy can, for simplicity, be parametrized by

$$\begin{aligned}
\varepsilon_{\mathrm{h}_1,\mathbf{k}} &= -\varepsilon_{\mathbf{k}} \ , \\
\varepsilon_{\mathrm{e}_1,\mathbf{k}} &= \varepsilon_{\mathbf{k}} - \delta_\mu + \delta_m \cos(2\theta) \ , \\
\varepsilon_{\mathrm{e}_2,\mathbf{k}} &= \varepsilon_{\mathbf{k}} - \delta_\mu - \delta_m \cos(2\theta) \ , \\
\varepsilon_{\mathrm{h}_2,\mathbf{k}} &= -\varepsilon_{\mathbf{k}} - E_M \ ,
\end{aligned} \tag{3}$$

close to the parameter regime of perfectly nested electron and hole bands which corresponds to $E_M = \delta_\mu = \delta_m = 0$. Here, we introduced $\varepsilon_{\mathbf{k}} = \frac{k^2}{2m} - \varepsilon_0$ and $\theta = \arctan(k_y/k_x)$. Note that changes of $\delta_\mu$ involve changes of the chemical potential, and therefore can be associated with doping, with $\delta_\mu = 0$ denoting perfect nesting. On the other hand, $\delta_m$ is a measure of the ellipticity of the electron bands. The top of the hole band at the $M$ point is lower in energy than the top of the hole band at the $\Gamma$ point, i.e. $E_M > 0$, such that it is not guaranteed to cross the Fermi surface even if it does exist. The respective noninteracting single-particle Green's functions are given by $G_{\lambda,\mathbf{k}}(\nu_n) = (\mathrm{i}\nu_n - \varepsilon_{\lambda,\mathbf{k}})^{-1}$ with $\nu_n = 2\pi T(n+1/2)$ being a fermionic Matsubara frequency.

The four-band model of the iron-based superconductors as introduced above allows for eleven fermionic interactions connecting the different parts of the Fermi surface, as discussed in Ref. 35. These interactions can be decomposed into different density-wave and pairing channels. Since in this work, we are concerned with magnetic order in these systems, we restrict ourselves to the contributions in the spin density wave channel,

$$\mathcal{H}_{\mathrm{int}} = -V \sum_{\mathbf{q}} \sum_{i,j} \mathbf{S}^{ij}_{\mathbf{q}} \cdot \mathbf{S}^{ij}_{-\mathbf{q}} \ , \tag{4}$$

$$\begin{aligned}
\text{where } \mathbf{S}^{ij}_{\mathbf{q}} = \sum_{\mathbf{k}} \sum_{\sigma_1,\sigma_2} \Big[ & c^\dagger_{\mathrm{h}_i,\mathbf{k},\sigma_1} \boldsymbol{\sigma}_{\sigma_1,\sigma_2} c_{\mathrm{e}_j,\mathbf{k}+\mathbf{q},\sigma_2} \\
& + c^\dagger_{\mathrm{e}_j,\mathbf{k},\sigma_1} \boldsymbol{\sigma}_{\sigma_1,\sigma_2} c_{\mathrm{h}_i,\mathbf{k}+\mathbf{q},\sigma_2} \Big] \ .
\end{aligned} \tag{5}$$

The interaction can be decoupled by means of a Hubbard-Stratonovich transformation upon which two magnetic order parameters arise, $\mathbf{M}_1$ and $\mathbf{M}_2$, associated with the two ordering vectors $\mathbf{Q}_1 = (\pi,0)$ and $\mathbf{Q}_2 = (0,\pi)$, respectively.

Their coupling to the electronic degrees of freedom on the mean-field level is given by

$$\begin{aligned}
\mathcal{H}_{\mathrm{int}}[\mathbf{M}_i] = & -\sum_{\mathbf{k},i} \mathbf{M}_i \cdot \left( c^\dagger_{\mathrm{e}_i,\mathbf{k},\sigma_1} \boldsymbol{\sigma}_{\sigma_1,\sigma_2} c_{\mathrm{h}_1,\mathbf{k},\sigma_2} + \mathrm{h.\,c.} \right) \\
& - \sum_{\mathbf{k},i} \mathbf{M}_i \cdot \left( c^\dagger_{\mathrm{h}_2,\mathbf{k},\sigma_1} \boldsymbol{\sigma}_{\sigma_1,\sigma_2} c_{\mathrm{e}_{\bar{i}},\mathbf{k},\sigma_2} + \mathrm{h.\,c.} \right)
\end{aligned} \tag{6}$$

where $\bar{i} = 2,1$ if $i = 1,2$. For details on the Hubbard-Stratonovich decoupling and the further derivation of the Ginzburg-Landau expansion, we refer to Appendix A. In the vicinity of the magnetic phase transition, we can integrate out the electronic degrees of freedom and derive the free energy expansion of the system

$$\begin{aligned}
F[\mathbf{M}_i] = & \sum_i a_i |\mathbf{M}_i|^2 + \sum_{i,j} u_{ij} |\mathbf{M}_i|^2 |\mathbf{M}_j|^2 \\
& + 2w (\mathbf{M}_1 \cdot \mathbf{M}_2)^2 \ ,
\end{aligned} \tag{7}$$

where the coefficients $a_i$, $u_{ij}$ and $w$ can be calculated from the microscopic model introduced above. Due to the rotational symmetry connecting the electron bands, it holds that $a_1 = a_2$, $u_{11} = u_{22}$, and $u_{12} = u_{21}$. The free energy (7) can thus be brought to the form of Eq. (1) using $u \equiv u_{12} + u_{11}$ and $g \equiv u_{12} - u_{11}$.

The transition temperature is determined by the quadratic part of the free energy. Since the $C_2 \leftrightarrow C_4$ transition is associated with a tricritical point, a corresponding kink in the transition temperature $T_{\mathrm{N}}$ is to be expected. The nature of the magnetic ground state, however, is solely determined by the interplay of the quartic coefficients $g$ and $w$ in this expansion as long as $u > \max(0, g, -w)$. Since our goal is to explain the formation of charge-spin density waves in a low-energy model of the FeSC, we are mainly interested in scenarios that yield $w < 0$. In the remainder of this section, we show that neglecting the incipient hole pocket at $M$ yields $w = 0$ in the clean case as a consequence of phase space restrictions. However, including the incipient pocket in a clean model leads to $w > 0$ and thus the spin-vortex crystal would be favorable. Only the inclusion of disorder can yield $w < 0$ and thus render the nonuniform charge-spin density wave order favorable.

### A. Clean three-band model

We start our considerations with the clean three-band model, i. e., disregarding the second hole pocket at the $M$ point which is not present in all FeSC compounds. The coefficients in the expansion of the free energy, previously defined in Ref. 26, are given by

$$\begin{aligned} a_i &= \frac{1}{4V} + 2\int_k G_{\mathrm{h}_\Gamma,\mathbf{k}}(\nu_n) G_{\mathrm{e}_i,\mathbf{k}}(\nu_n) \ , \\ u &= \frac{1}{2}\int_k G^2_{\mathrm{h}_\Gamma,\mathbf{k}}(\nu_n)[G_{\mathrm{e}_1,\mathbf{k}}(\nu_n) + G_{\mathrm{e}_2,\mathbf{k}}(\nu_n)]^2 \ , \\ g &= -\frac{1}{2}\int_k G^2_{\mathrm{h}_\Gamma,\mathbf{k}}(\nu_n)[G_{\mathrm{e}_1,\mathbf{k}}(\nu_n) - G_{\mathrm{e}_2,\mathbf{k}}(\nu_n)]^2 \ , \\ w &= 0 \ , \end{aligned} \tag{8}$$

where we abbreviated $\int_k \ldots \equiv T\sum_n \int \frac{\mathrm{d}\mathbf{k}}{(2\pi)^2} \ldots$ For convenience, we write $u$ and $g$ here in the symmetrized form, namely $u = \frac{1}{2}(u_{11} + u_{12} + u_{21} + u_{22})$ and $g = -\frac{1}{2}(u_{11} - u_{12} - u_{21} + u_{22})$. The coefficient $w$ vanishes in the clean model as a consequence of the trace in spin space[34]: The most generic quartic diagram [see Fig. 3(a)] is proportional to

$$\begin{aligned} &\mathrm{tr}\left[\sum_{ijkl} M^{(i)}_{\lambda_1}\sigma_i M^{(j)}_{\lambda_2}\sigma_j M^{(k)}_{\lambda_3}\sigma_k M^{(l)}_{\lambda_4}\sigma_l\right] \\ &= 2\big[(\mathbf{M}_{\lambda_1}\cdot\mathbf{M}_{\lambda_2})(\mathbf{M}_{\lambda_3}\cdot\mathbf{M}_{\lambda_4}) \\ &\quad - (\mathbf{M}_{\lambda_1}\cdot\mathbf{M}_{\lambda_3})(\mathbf{M}_{\lambda_2}\cdot\mathbf{M}_{\lambda_4}) \\ &\quad + (\mathbf{M}_{\lambda_1}\cdot\mathbf{M}_{\lambda_4})(\mathbf{M}_{\lambda_2}\cdot\mathbf{M}_{\lambda_3})\big] \ . \end{aligned} \tag{9}$$

Within the minimal model, introduced in Eqs. (2) and (6), and with the additional simplification of neglecting the pocket at the $M$ point, the absence of scattering as well as interactions between the electron bands require that either $\lambda_1 = \lambda_2$ and $\lambda_3 = \lambda_4$, or $\lambda_1 = \lambda_4$ and $\lambda_2 = \lambda_3$ holds, as can be seen from Fig. 3(a). Both conditions result in $\mathrm{tr}[(\mathbf{M}_{\lambda_1}\cdot\boldsymbol{\sigma})(\mathbf{M}_{\lambda_2}\cdot\boldsymbol{\sigma})(\mathbf{M}_{\lambda_3}\cdot\boldsymbol{\sigma})(\mathbf{M}_{\lambda_4}\cdot\boldsymbol{\sigma})] = 2|\mathbf{M}_{\lambda_1}|^2|\mathbf{M}_{\lambda_3}|^2$ and thus imply $w = 0$ in the clean case. On the contrary, the inclusion of interband scattering or interactions between the two electron pockets at $\mathbf{Q}_1$ and $\mathbf{Q}_2$ allows for contributions where $\lambda_1 = \lambda_3$ and $\lambda_2 = \lambda_4$, rendering $w$ finite since then $\mathrm{tr}[(\mathbf{M}_{\lambda_1}\cdot\boldsymbol{\sigma})(\mathbf{M}_{\lambda_2}\cdot\boldsymbol{\sigma})(\mathbf{M}_{\lambda_3}\cdot\boldsymbol{\sigma})(\mathbf{M}_{\lambda_4}\cdot\boldsymbol{\sigma})] = 2\left[2(\mathbf{M}_{\lambda_1}\cdot\mathbf{M}_{\lambda_2}) - |\mathbf{M}_{\lambda_1}|^2|\mathbf{M}_{\lambda_2}|^2\right]$.

### B. Incipient hole pocket at the $M$ point

The inclusion of an incipient hole pocket at $(\pi,\pi)$ allows for contributions that render $w$ finite in an analogous manner. The contribution to the planar coupling $w$ that survives the spin trace as a consequence of the presence of the second hole pocket is depicted diagrammatically in Fig. 3(b). We consider the simplest case where $\delta_\mu = \delta_m = 0$, i. e., perfect nesting of the hole band at the $\Gamma$ point and the two electron bands, since this yields a finite value for the planar coupling,

$$w \approx \begin{cases} \frac{7\rho_\mathrm{F}\zeta(3)}{2\pi^2T^2} \approx 0.43\frac{\rho_\mathrm{F}}{T^2} & , \quad E_M \ll T \ , \\ \frac{4\rho_\mathrm{F}}{E_M^2} & , \quad E_M \gg T \ , \end{cases} \tag{10}$$

where $\zeta(z)$ is the Riemann zeta function, and we assumed the density of states at the Fermi level to be given by a constant $\rho_\mathrm{F}$ in all bands. For more details on the calculation of the coefficients, we refer to Appendix B.

Hence we find that the inclusion of the second hole pocket indeed lifts the degeneracy of the two double-$\mathbf{Q}$ magnetically ordered states. However, it can only account for the formation of a spin-vortex crystal since $w > 0$ always. Furthermore, if the pocket at $M$ is shifted to energies far below the Fermi level, we reproduce the results of the previously discussed three-band model since the coefficient $w$ vanishes in the limit $E_M \to \infty$, which is the relevant limit for many of the FeSC compounds.

A positive planar coupling $w > 0$ has also been obtained in previous studies of other extensions of the clean three-band model such as the perturbative inclusion of additional interactions.[19,22] This suggests a different route to $w < 0$ is needed in order to explain the formation of the collinear CSDW state within this low-energy model. Consequently, in the remainder of this paper, we investigate the effect of disorder on the magnetic ground state. Furthermore, we neglect the hole pocket at the $M$ point since it is not a generic feature of the FeSC family and its inclusion is not able to explain why the nonuniform CSDW is favored over the noncollinear SVC in the hole-doped compounds.

### C. Impurity scattering

Impurity scattering will affect both the magnetic transition temperature, determined by the vanishing of $a$, and the nature of the magnetic ground state, determined by $g$ and $w$. Hereafter, we focus on the latter effect – the former gives rise to a suppression of the magnetic transition

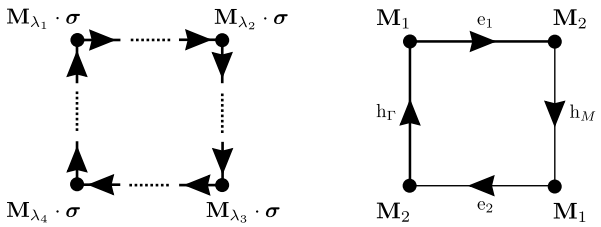


(a) generic diagram before performing the spin trace

(b) contribution to $w$ in a clean four-band model

FIG. 3. Quartic diagrams in the absence of disorder. (a) Sketch of a generic quartic diagram before performing the spin trace: Each vertex couples the hole band to one of the electron bands, and the dashed lines indicate that scattering or additional interactions could alter the diagram. (b) Contribution to the planar coupling constant $w$ if the incipient hole pocket at $M$ is taken into account.

temperature with disorder, as shown elsewhere[10,36]. In the particle-hole symmetric case (perfect nesting), where $\delta_\mu = \delta_m = 0$, the nematic coupling constant $g$ vanishes. Finite ellipticity $\delta_m \neq 0$, however, causes $g$ to be finite. The effect of doping can then partially be accounted for by a finite value of the chemical potential, i. e., $\delta_\mu \neq 0$.

Meanwhile, doping also introduces disorder, which has a different effect on the electronic structure than the rigid band shift assumed by changing the chemical potential.[37] For instance, it has been shown that impurity scattering can locally stabilize charge-spin density wave order,[29] thus suggesting that the inclusion of disorder for the itinerant electrons participating in the formation of the magnetically ordered state is an important ingredient for the investigation of the CSDW state. Hence we consider an arbitrary realization of nonmagnetic impurities, thus adding the term

$$\mathcal{H}_{\mathrm{dis}} = \sum_{\lambda,\lambda'} \sum_{\mathbf{k},\mathbf{k}'} \sum_{\sigma} c^\dagger_{\lambda,\mathbf{k},\sigma} W_{\lambda\lambda'}(\mathbf{k},\mathbf{k}') c_{\lambda',\mathbf{k}',\sigma} \tag{11}$$

to the Hamiltonian. As usual, we are not interested in quantities that depend on the microscopic disorder realization, but rather in self-averaged physical observables. Therefore, we are interested in disorder-averaged quantities where all information about the disorder is encoded in the correlation function

$$\begin{aligned} &\left\langle W_{\lambda_1\lambda_1'}(\mathbf{k}_1,\mathbf{k}_1') W_{\lambda_2\lambda_2'}(\mathbf{k}_2,\mathbf{k}_2') \right\rangle_{\mathrm{dis}} \\ &= \Gamma_{\lambda_1\lambda_1'\lambda_2\lambda_2'}(\mathbf{k}_1,\mathbf{k}_1',\mathbf{k}_2,\mathbf{k}_2') \delta(\mathbf{k}_1+\mathbf{k}_2-\mathbf{k}_1'-\mathbf{k}_2'+\mathbf{K}) \end{aligned} \tag{12}$$

where $\langle \ldots \rangle_{\mathrm{dis}}$ denotes the average over disorder configurations which restores translation invariance, and $\mathbf{K}$ is a vector from the reciprocal lattice. Thus the correlator constitutes a measure of impurity strength and is proportional to the scattering rate $\Gamma$ characterizing the respective scattering process. These scattering rates depend on the impurity concentration as well as on the strength of the disorder potential itself. In the diagrams contributing to the coefficients of the Ginzburg-Landau expansion in the presence of disorder, discussed in the subsequent chapters, this impurity correlation function is depicted as a dashed line.

In the remainder, we concentrate on the simplest type of impurities and thus assume the disorder to be sufficiently smooth on the individual sheets of the Fermi surface such that the momentum dependence of the scattering rates can be neglected for momenta from the same pocket of the Fermi surface. Then, scattering within one band or between two bands is characterized by constant scattering rates $\Gamma_{\mathrm{e}}^{\mathrm{intra}}$, $\Gamma_{\mathrm{h}}^{\mathrm{intra}}$ or $\Gamma_{\mathrm{e-e}}^{\mathrm{inter}}$, $\Gamma_{\mathrm{e-h}}^{\mathrm{inter}}$, respectively. Here we assume that both electron bands are affected in the same way by impurities, and thus the respective scattering rates are equal – consistent with the tetragonal symmetry of the system. Note that in a multiband model, the effect of impurity scattering can have subtle consequences[38] which we avoid here by requiring that all scattering processes be characterized by real numbers, i. e., the impurities do not break time-reversal invariance locally. Furthermore, we assume the impurity potential to be sufficiently weak such that single-particle interference effects can be neglected. In this case, calculating the self-energy within the Born approximation is appropriate, resulting in

$$G_{\lambda,\mathbf{k}}(\nu_n) = \frac{1}{\mathrm{i}\nu_n - \varepsilon_{\lambda,\mathbf{k}} + \frac{\mathrm{i}}{2\tau_\lambda}\,\mathrm{sgn}(\nu_n)} \tag{13}$$

for the propagator in band $\lambda$ in the presence of impurities. Here, we introduced the elastic scattering time

$$\tau_\lambda = (2\pi\rho_{\mathrm{F}}\Gamma_{\mathrm{total}})^{-1}, \tag{14}$$

which is determined by the total scattering rate including all intraband and interband scattering processes that affect propagation of electrons in band $\lambda$.

## III. RESULTS

In multiband systems, the interplay of a multitude of different intraband and interband scattering processes can affect physical properties. Fortunately, in the iron-based systems, experiments as well as ab-initio calculations reveal that not all of them are equally important.[39–46] This allows us to devise models of impurity scattering that concentrate on the dominant scattering processes relevant for the calculation of $g$, $u$, and $w$. Such a simplification allows us to draw conclusions about the dominant effects that are to be expected due to impurity scattering, but of course restricts exact quantitative predictions.

For many aspects, it is sufficient to discriminate between intraband and interband scattering processes, and thus it is important to note that interband scattering (which for example causes pair breaking in the superconducting state) is much weaker than the dominant intraband scattering process affecting transport properties.[39–41] Furthermore, as demonstrated by transport measurements,[42,43] scanning tunneling microscopy,[44] and first-principles density functional theory calculations,[45,46] the intraband scattering rate in the hole band exceeds the intraband scattering rate in the electron bands. For these reasons, we consider the following hierarchy of scattering rates in the remainder of the paper:

$$\Gamma_{\mathrm{e-e}}^{\mathrm{inter}}, \Gamma_{\mathrm{e-h}}^{\mathrm{inter}}, \Gamma_{\mathrm{e}}^{\mathrm{intra}} \ll \Gamma_{\mathrm{h}}^{\mathrm{intra}} \,. \tag{15}$$

The main advantage of the minimal three-band model of Section II A is that it allows for a well-defined perturbative expansion near the perfect-nesting limit ($\delta_\mu = \delta_m = 0$) and the clean limit ($\Gamma_i = 0$), since in this case $g = w = 0$, and the degeneracy of the magnetic ground state is maximal (i.e. the stripe-magnetic, CSDW, and SVC phases are all degenerate). Therefore, one can assess qualitatively how different types of perturbations favor distinct ground states.

### A. Effect of disorder on the nematic coupling $g$

We first analyze how disorder affects $g$, since this coupling constant determines whether the system condenses in a single-**Q** or double-**Q** state. While $g = 0$ at perfect nesting, the nematic coupling constant takes a finite value within the three-band model as a consequence of the ellipticity of the electron bands; although orbital dressing effects can make it nonzero even at perfect nesting[47]. Focusing on the contribution from the dominant scattering rate $\Gamma_{\mathrm{h}}^{\mathrm{intra}}$, see Eq. (15), and expanding near perfect nesting, $\delta_\mu, \delta_m \ll 2\pi T$, we find

$$g = -\frac{\rho_{\mathrm{F}}\delta_m^2}{1536\pi^4 T^4}\left[\psi_4\left(\frac{1}{2}+\frac{\rho_{\mathrm{F}}\Gamma_{\mathrm{h}}^{\mathrm{intra}}}{4T}\right) - \frac{\delta_\mu^2}{32\pi^2T^2}\,\psi_6\left(\frac{1}{2}+\frac{\rho_{\mathrm{F}}\Gamma_{\mathrm{h}}^{\mathrm{intra}}}{4T}\right)\right], \tag{16}$$

where $\psi_n(z)$ is the $n^{\mathrm{th}}$ derivative of the digamma function. For more details on how to evaluate the coefficients, see Appendix B. The contributing diagrams $\mathcal{G}_i^{(1)}$ and $\mathcal{G}_i^{(2)}$ are depicted in Fig. 4(a) and (b), and correspond to the disorder-induced Green's function renormalization and to the vertex correction, respectively. Here, we used that $u_{11} = u_{22}$ and $u_{12} = u_{21}$ holds for the quartic coefficients in the expansion (7) also in the presence of disorder, and that $\mathcal{G}_2^{(2)} - \mathcal{G}_1^{(2)} \propto \int \frac{\mathrm{d}\theta}{2\pi}\cos(2\theta) = 0$.

In the clean limit where $\Gamma_{\mathrm{h}}^{\mathrm{intra}} = 0$, $g \propto \delta_m^2$ changes sign from positive to negative for sufficiently large $\delta_\mu/(2\pi T)$, as shown in Fig. 2(a) and in agreement with previous results[19]. This describes the transition from a single-**Q** to a double-**Q** magnetic ground state as the carrier concentration increases. We note that the resulting coefficient is dependent on $\delta_\mu^2$ rather than on $\delta_\mu$, thus yielding the same results for electron and hole doping. However, a more realistic band structure indeed results in an electron-hole asymmetry of the coupling constant $g$, see Ref. 48, in accordance with experiments where the $C_4$-magnetic phase has only been observed for hole-doped compounds so far.

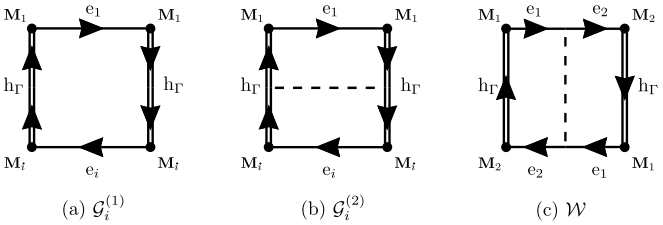


FIG. 4. Leading-order diagrams contributing to the quartic coefficients that determine the magnetic ground state. Double lines indicate that the respective propagators acquire a finite lifetime due to impurity scattering whereas single lines are used for propagators in bands that, within our model, are not affected by impurity scattering. Additional scattering processes in (b) and (c) are indicated by a dashed line corresponding to the scattering rates $\Gamma_{\mathrm{h}}^{\mathrm{intra}}$ and $\Gamma_{\mathrm{e-e}}^{\mathrm{inter}}$, respectively. (a) and (b) $\mathcal{G}_i^{(1)}$ and $\mathcal{G}_i^{(2)}$ ($i \in \{1,2\}$) are the contributions to $g$ (as well as to $u$) in the presence of intraband scattering in the hole band which is the dominant scattering mechanism in FeSC. (c) $\mathcal{W}$ is the contribution to $w$ which is finite owing to interband scattering between the two electron bands, and in the presence of the dominant intraband scattering in the hole band.

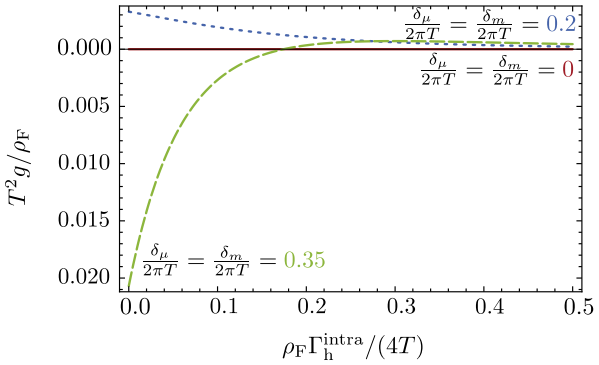


FIG. 5. Nematic coupling constant $g$ in the presence intraband scattering in the hole band, characterized by the scattering rate $\Gamma_{\mathrm{h}}^{\mathrm{intra}}$. We chose $\delta_\mu/(2\pi T) = \delta_m/(2\pi T) = 0.2$ (blue, dotted line) as an example of small ellipticity and detuning which guarantees $w < 0$ and $g > 0$, and $\delta_\mu/(2\pi T) = \delta_m/(2\pi T) = 0.35$ (green, dashed line) as an example where disorder can tune $g$ and $w$ to be either positive or negative. The red line represents the result at particle-hole symmetry, $\delta_\mu/(2\pi T) = \delta_m/(2\pi T) = 0$.

The resulting coupling constant $g$ as a function of the scattering rate $\Gamma_{\mathrm{h}}^{\mathrm{intra}}$, plotted for different values of detuning $\delta_\mu$ and ellipticity $\delta_m$, is shown in Fig. 5. In the particle-hole symmetric case, $g = 0$ as a consequence of $\delta_m = 0$, regardless of whether the system is in the clean or dirty limit. Interestingly, if $g$ is positive (negative) in the clean limit, the addition of disorder suppresses $g$ and can even induce a sign-change. Therefore, the transition from a single-**Q** to a double-**Q** state can be controlled not only by carrier concentration, but also by the disorder potential.

Even when the suppression of $g$ by disorder does not induce a sign-change, it has important consequences for the phase diagram. In particular, as shown in Ref. 26, the splitting $\Delta T = T_{\mathrm{s}} - T_{\mathrm{N}}$ between the nematic/structural and the magnetic transitions is controlled by the inverse dimensionless nematic coupling constant $u/g$ and the dimensionality $d$. In particular, for $2 < d < 3$, which mimics an anisotropic 3D system, the two transitions are simultaneous and first order for $(u/g) < (u/g)_{c_1} = 1/(3-d)$. For $(u/g)_{c_1} < (u/g) < (u/g)_{c_2}$, the transitions are split and one of them remains first-order whereas the other transition is second-order. In this regime, an increase in $u/g$ results in an enhanced splitting $\Delta T$, whereas deep in the regime of two split second-order phase transitions, $(u/g) \gg (u/g)_{c_2} = (6-d)/(6-2d)$, increasing the ratio $u/g$ reduces the splitting $\Delta T$. To

compute the dimensionless parameter $u/g$, we compute $u$ analogously to the case of $g$,

$$u = -\frac{\rho_F}{8\pi^2 T^2}\Big[\psi_2\left(\frac{1}{2}+\frac{\rho_F\Gamma_h^{\rm intra}}{4T}\right) \tag{17}$$

$$+\frac{\rho_F\Gamma_h^{\rm intra}}{12T}\,\psi_3\left(\frac{1}{2}+\frac{\rho_F\Gamma_h^{\rm intra}}{4T}\right)\Big] \tag{18}$$

$$+\frac{\rho_F}{768\pi^4T^4}\,\psi_4\left(\frac{1}{2}+\frac{\rho_F\Gamma}{4T}\right)\left[3\delta_\mu^2+\delta_m^2\right] \tag{19}$$

$$+\frac{\rho_F^2\Gamma_h^{\rm intra}}{30720\pi^4T^5}\,\psi_5\left(\frac{1}{2}+\frac{\rho_F\Gamma}{4T}\right)\left[10\delta_\mu^2+3\delta_m^2\right] \tag{20}$$

in accordance with previous work.[49] Near particle-hole symmetry, where $\delta_\mu/(2\pi T)$ and $\delta_m/(2\pi T)$ are sufficiently small, and the magnetic ground state is the stripe one, $g/u$ decreases monotonically with increasing scattering rate as shown in Fig. 6(a). Thus, if the system initially is near the regime of first-order simultaneous transitions, as it is the case in undoped $BaFe_2As_2$, the addition of disorder is expected to cause (or enhance) a splitting in the magnetic and structural transitions. This agrees with recent experiments in $BaFe_2As_2$, which observed enhanced splitting of the transitions upon electron irradiation.[9] This result is also consistent with the theoretical finding of Ref. 10 that disorder stabilizes the nematic phase. We note, however, that the dependence of the ratio $g/u$ on disorder is nonuniversal [see Fig. 6(b) and (c)]. In particular, further away from particle-hole symmetry, the dependence of $g/u$ on disorder is no longer monotonic: $g/u$ first increases with increasing scattering rate, and above a critical value starts decreasing again.

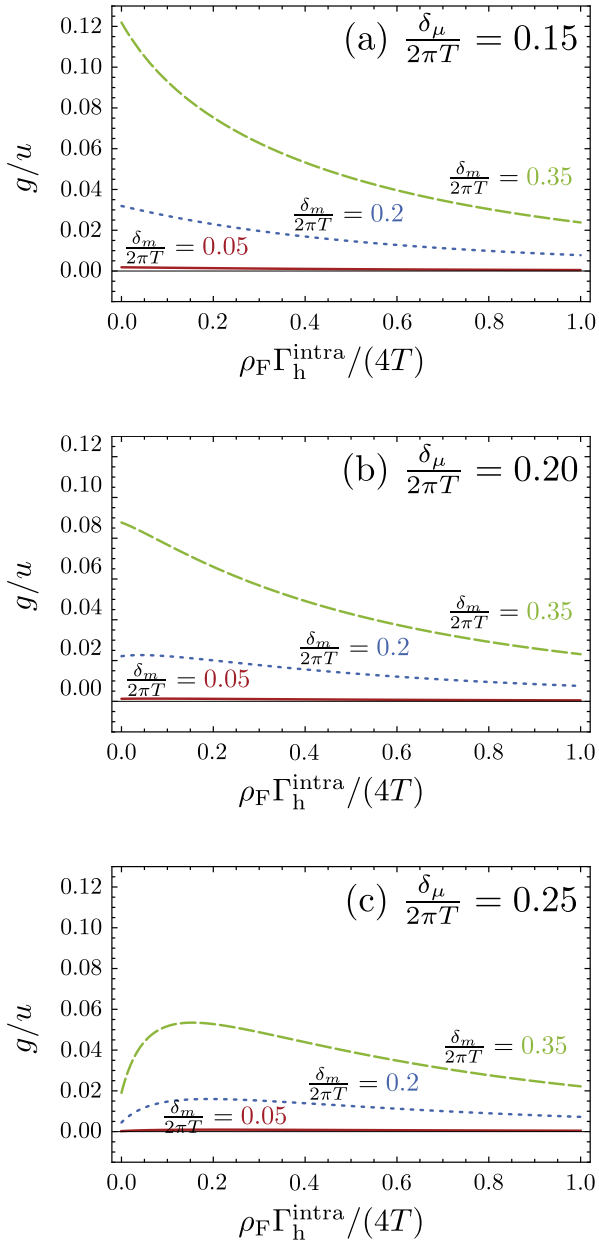


FIG. 6. Dependence of the dimensionless nematic coupling constant $g/u$ on disorder. (a) Close to particle-hole symmetry, $g/u$ decreases monotonically with increasing scattering rate. (b) and (c) With increasing distance to particle-hole symmetry, an initial increase of the dimensionless nematic coupling constant is found for small scattering rates, but for stronger disorder, the ratio $g/u$ decreases again.

### B. Effect of disorder on the planar coupling $w$

Having established that $g$ can become either positive or negative in both clean and dirty systems, we now analyze $w$. As discussed above and illustrated in Fig. 3(a), in the clean three-band model $w = 0$ always. Following the analysis of the generic fourth-order diagram in Fig. 3 and Eq. (9), the only scattering processes that gives rise to a nonzero contribution to $w$ is the one that couples the electron pocket at $\mathbf{Q}_1$ and the electron pocket at $\mathbf{Q}_2$, characterized by the scattering rate $\Gamma_{e-e}^{\rm inter}$. For the sake of clarity, we neglect all other interband scattering processes since they give subleading contributions to $w$, i.e. $w = 0$ always as long as $\Gamma_{e-e}^{\rm inter} = 0$. Then, in the presence of the dominant scattering process, intraband scattering in the hole band and, additionally, interband scattering between the electron bands, we find

$$w = -\frac{\rho_F^2\Gamma_{e-e}^{\rm inter}}{96\pi^2T^3}\left[\psi_3\left(\frac{1}{2}+\frac{\rho_F(\Gamma_h^{\rm intra}+\Gamma_{e-e}^{\rm inter})}{4T}\right)\right.$$
$$\left.-\frac{10\delta_\mu^2+\delta_m^2}{320\pi^2T^2}\,\psi_5\left(\frac{1}{2}+\frac{\rho_F(\Gamma_h^{\rm intra}+\Gamma_{e-e}^{\rm inter})}{4T}\right)\right], \tag{21}$$

where we assumed the density of states at the Fermi surface to be given by a constant $\rho_F$ in all three bands, and we expanded to leading order in $\delta_\mu/(2\pi T)$ and $\delta_m/(2\pi T)$ to obtain the results. The respective diagram denoted by $\mathcal{W}$ is depicted in Fig. 4(c). Note that contributions with more than one scattering process between electron bands vanish upon momentum integration and thus the above result already includes contributions up to infinite order

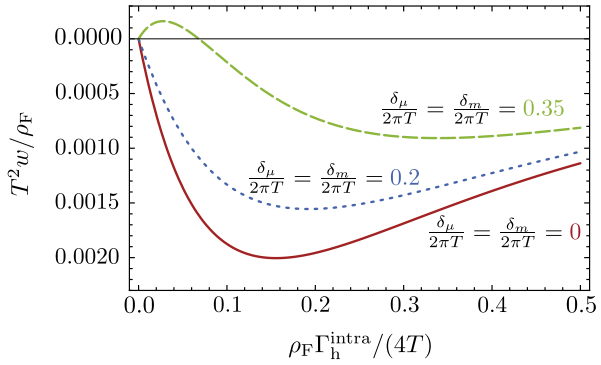


FIG. 7. Planar coupling $w$ as a function of intraband scattering rate in the hole band, $\Gamma_h^{intra}$, where we set $\Gamma_{e-e}^{inter} = 0.1\Gamma_h^{intra}$. We chose $\delta_\mu/(2\pi T) = \delta_m/(2\pi T) = 0.2$ (blue, dotted line) as an example of small ellipticity and detuning which guarantees $w < 0$ and $g > 0$, and $\delta_\mu/(2\pi T) = \delta_m/(2\pi T) = 0.35$ (green, dashed line) as an example where disorder can tune $w$ and $g$ to be either positive or negative. The red line represents the result at particle-hole symmetry, $\delta_\mu/(2\pi T) = \delta_m/(2\pi T) = 0$.

in $\Gamma_{e-e}^{inter}$.

We show the coefficient $w$ as a function of the scattering rate for different values of detuning $\delta_\mu$ and ellipticity $\delta_m$ in Fig. 7. In the absence of impurity scattering, we recover $w = 0$. At particle-hole symmetry, $\delta_\mu = \delta_m = 0$, disorder leads to $w < 0$, thus favoring the formation of a charge-spin density wave [see Fig. 1(a)] as long as $g < |w|$. In contrast, finite detuning and ellipticity yield a contribution of opposite sign and thus, depending on the scattering rate and the distance from particle-hole symmetry, $w$ can be either positive or negative, allowing for both proposed double-**Q** states, CSDW and the SVC. This conclusion holds also in the presence of magnetic impurities. In this case, however, the global prefactor and the total scattering rate are altered as compared to the case of nonmagnetic impurities since for magnetic impurities, the evaluation of the trace $\mathrm{tr}[\sigma_i\sigma_j\sigma_k\sigma_l\sigma_j\sigma_m]$ allows for additional contributions including other interband scattering processes between the electron pockets $e_1$ and $e_2$.

## IV. SUMMARY AND CONCLUSIONS

Recent experiments revealed the existence of $C_4$-magnetic phases in hole-doped iron-based superconductors, further fueling the discussion about the nature of the magnetic ground state of the parent compounds. We considered a three-band model of iron-based superconductors complemented by an incipient fourth pocket at the $M$ point and investigated how the interplay of impurity scattering and disorder effects in a rigid-band approach affects the magnetic ground state.

The phase diagram is governed by the interplay of nematic and planar couplings, $g$ and $w$, respectively. If $g > \max(0, -w)$, stripe-magnetic order with either $\mathbf{M}_1 = 0$ or $\mathbf{M}_2 = 0$ is favored, as it has been observed in many compounds of the iron pnictide and iron chalcogenide families. If $g < \max(0, -w)$, a double-**Q** state with $|\mathbf{M}_1| = |\mathbf{M}_2|$ minimizes the free energy, and the sign of $w$ determines whether $\mathbf{M}_1 \perp \mathbf{M}_2$ (spin-vortex crystal, for $w > 0$) or $\mathbf{M}_1 = \pm\mathbf{M}_2$ (charge-spin density wave, for $w < 0$) is more favorable. So far, only the charge-spin density wave has been observed experimentally,[18,31,32] in contrast to theoretical models.[19,22,33]

Although generic three-band low-energy models for the description of FeSC allow for $C_4$-magnetic ground states, they leave the spin-vortex crystal (SVC) and the charge-spin density wave (CSDW) degenerate since $w = 0$. Our analysis shows that the existence of an incipient pocket at $(\pi, \pi)$ lifts the degeneracy, however, it would favor the formation of a spin-vortex crystal ($w > 0$) and thus cannot explain the experimental findings. The investigation of other extensions to the three-band model such as the consideration of additional interactions has lead to the same conclusion that the SVC state is favorable.

Our investigation of impurity scattering, in contrast, provides a natural explanation for the formation of a charge-spin density wave in doped FeSC. Since the three-band model under consideration yields $w = 0$ in the absence of impurity scattering, we concentrated on the interband scattering process between the two electron bands that can render $w$ finite. In addition, we considered the dominant impurity scattering process in FeSC which is intraband scattering in the hole band. We find $w < 0$ at particle-hole symmetry as well as for small ellipticity and detuning, suggesting that disorder can promote charge-spin density waves. However, sufficiently large ellipticity and detuning in combination with impurity scattering also allow for $w > 0$, i. e., a spin-vortex crystal.

Our findings are summarized in the phase diagrams depicted in Fig. 2 where we show the magnetic ground states that are favored in different regimes of detuning and ellipticity. Disorder favors the double-**Q** charge-spin density wave over the single-**Q** stripe-magnetic SDW at small ellipticity and detuning, and increasing scattering rate increases the parameter regime in which CSDW order is expected to occur.

We further investigated the effect of the dominant impurity scattering process in FeSC, intraband scattering in the hole band, on the nematic coupling $g$, which in the three-band model assumes a finite value as long as the electron bands exhibit finite ellipticity. In the absence of impurity scattering and for $\delta_\mu = 0$, $g$ is positive, and increasing intraband scattering in the hole band reduces the nematic coupling constant, concordant with the experimental finding that electron irradiation enhances the splitting between structural and magnetic transition in the stripe-ordered phase.

Previously, controlled disorder has been proposed as a way to tune the properties of the superconducting state in the iron-based materials.[50] Analogously, our findings

provide a promising control knob to tune their magnetic ground state. In particular, addition of impurities via electron irradiation in hole-doped compounds near the composition where the single-**Q** to double-**Q** magnetic transition is observed could stabilize a $C_4$-magnetic phase as the leading instability of the system – currently, the $C_4$-magnetic phase has been mostly observed inside the $C_2$-magnetic phase boundary. Similarly, removal of impurities via annealing in samples that display the double-**Q** magnetic order could change the nature of the $C_4$ phase from charge-spin density wave to spin-vortex crystal.

## ACKNOWLEDGMENTS

We thank E. Berg, M. Christensen, A. Chubukov, I. Eremin, J. Kang, S. Kivelson, M. S. Scheurer, and X. Wang for helpful discussions. M.H. and J.S. are supported by the Deutsche Forschungsgemeinschaft through DFG-SPP 1458 'Hochtemperatursupraleitung in Eisenpniktiden'. A.L. acknowledges support by NSF Grant No. DMR-1606517 and in part by DAAD grant from German Academic Exchange Services. Support for this research at the University of Wisconsin-Madison was provided by the Office of the Vice Chancellor for Research and Graduate Education with funding from the Wisconsin Alumni Research Foundation. R.M.F. is supported by the U.S. Department of Energy, Office of Science, Basic Energy Sciences, under award number DE-SC0012336.

## Appendix A: Microscopic calculation of the Ginzburg-Landau coefficients

In this appendix, we present details on the derivation of the Ginzburg-Landau expansion of the free energy in terms of the magnetic order parameters $\mathbf{M}_1$ and $\mathbf{M}_2$, starting from the partition function $\mathcal{Z} = \int \mathcal{D}[\bar{\psi}, \psi] \mathrm{e}^{-\mathcal{S}[\bar{\psi},\psi]}$. The action $\mathcal{S}[\bar{\psi}, \psi]$ corresponding to the Hamiltonian $\mathcal{H} = \mathcal{H}_0 + \mathcal{H}_{\mathrm{int}}$ as introduced in Eqs. (2) and (5) is given by

$$\mathcal{S}[\bar{\psi}, \psi] = \int_0^\beta \mathrm{d}\tau \sum_{\lambda,\mathbf{k},\sigma} \bar{\psi}_{\lambda,k,\sigma} \partial_\tau \psi_{\lambda,k,\sigma} + \mathcal{H}[\bar{\psi}, \psi] \ , \tag{A1}$$

where $\bar{\psi}$ and $\psi$ are fermionic field operators, and $\lambda$ labels the four bands. We switch to Matsubara frequency and momentum space, where the action can be written as

$$\mathcal{S}[\bar{\psi}, \psi] = \mathcal{S}_0[\bar{\psi}, \psi] + \mathcal{S}_{\mathrm{int}}[\bar{\psi}, \psi] \ , \tag{A2}$$

$$\text{where} \quad \mathcal{S}_0[\bar{\psi}, \psi] = \sum_{\lambda,k,\sigma} \bar{\psi}_{\lambda,k,\sigma} (-\mathrm{i}\nu_n + \epsilon_{\lambda,\mathbf{k}}) \psi_{\lambda,k,\sigma} \ , \tag{A3}$$

$$\begin{aligned} \mathcal{S}_{\mathrm{int}}[\bar{\psi}, \psi] = -V \sum_{i,j} \sum_{k,k',q} \sum_{\sigma_1,\ldots,\sigma_4} & \left[ \bar{\psi}_{\mathrm{h}_i,k,\sigma_1} \boldsymbol{\sigma}_{\sigma_1\sigma_2} \psi_{\mathrm{e}_j,k+q,\sigma_2} + \bar{\psi}_{\mathrm{e}_i,k,\sigma_1} \boldsymbol{\sigma}_{\sigma_1\sigma_2} \psi_{\mathrm{h}_j,k+q,\sigma_2} \right] \\ & \cdot \left[ \bar{\psi}_{\mathrm{h}_i,k,\sigma_3} \boldsymbol{\sigma}_{\sigma_3\sigma_4} \psi_{\mathrm{e}_j,k-q,\sigma_4} + \bar{\psi}_{\mathrm{e}_i,k,\sigma_3} \boldsymbol{\sigma}_{\sigma_3\sigma_4} \psi_{\mathrm{h}_j,k-q,\sigma_4} \right] \ , \end{aligned} \tag{A4}$$

where we introduced the notation $k \equiv (\mathrm{i}\nu_n, \mathbf{k})$ and $\int_k \ldots = T \sum_n \sum_{\mathbf{k}} \ldots$ for brevity. The interaction term of the action, $\mathrm{e}^{-\mathcal{S}_{\mathrm{int}}}$ can be decoupled by introducing a real, three-component vector field $\mathbf{M}_q$ via a Hubbard-Stratonovich transformation,

$$\mathrm{e}^{-\mathcal{S}_{\mathrm{int}}[\bar{\psi},\psi]} = \int \mathcal{D}\mathbf{M} \, \mathrm{e}^{-\mathcal{S}_{\mathrm{int}}[\mathbf{M},\bar{\psi},\psi]} \ , \tag{A5}$$

$$\begin{aligned} \text{where} \quad \mathcal{S}_{\mathrm{int}}[\mathbf{M}, \bar{\psi}, \psi] = \frac{1}{4V} \sum_i \int_q \mathbf{M}_{i,q} \cdot \mathbf{M}_{i,-q} - \sum_i \sum_{\sigma_1,\sigma_2} \int_{k,q} \mathbf{M}_{1,q} \cdot \boldsymbol{\sigma}_{\sigma_1,\sigma_2} \left[ \bar{\psi}_{\mathrm{h}_i,k,\sigma_1} \psi_{\mathrm{e}_i,k-q,\sigma_2} + \bar{\psi}_{\mathrm{e}_i,k,\sigma_1} \psi_{\mathrm{h}_i,k-q,\sigma_2} \right] \\ - \sum_i \sum_{\sigma_1,\sigma_2} \int_{k,q} \mathbf{M}_{2,q} \cdot \boldsymbol{\sigma}_{\sigma_1,\sigma_2} \left[ \bar{\psi}_{\mathrm{h}_i,k,\sigma_1} \psi_{\mathrm{e}_{\bar{i}},k-q,\sigma_2} + \bar{\psi}_{\mathrm{e}_{\bar{i}},k,\sigma_1} \psi_{\mathrm{h}_i,k-q,\sigma_2} \right] \ , \end{aligned} \tag{A6}$$

where we abbreviated $\mathbf{M}_{i,q} = \mathbf{M}_{Q_i+q}$ introducing the ordering vectors $\mathbf{Q}_1 = (0,\pi)$ and $\mathbf{Q}_2 = (\pi,0)$. We introduce the spinor $\bar{\Psi}_k = \left(\bar{\psi}_{\mathrm{h}_1,k} \;\; \bar{\psi}_{\mathrm{e}_1,k} \;\; \bar{\psi}_{\mathrm{e}_2,k} \;\; \psi_{\mathrm{h}_2,k}\right)$ in order to write the action in the compact form

$$\mathcal{S}[\mathbf{M},\bar{\Psi},\Psi] = \frac{1}{4V}\sum_i \int_q \mathbf{M}_{i,q}\mathbf{M}_{i,-q} - \int_{k,k'} \bar{\Psi}_k \mathcal{G}^{-1}_{k,k'} \Psi_{k'} \tag{A7}$$

$$\text{with the matrix} \quad \mathcal{G}^{-1}_{k,k'} = \mathcal{G}^{-1}_{0;k,k'} + \mathcal{V} \;, \tag{A8}$$

$$\text{where} \quad \mathcal{G}^{-1}_{0;k,k'} = \delta_{k,k'} \begin{pmatrix} G^{-1}_{\mathrm{h}_1,k} & 0 & 0 & 0 \\ 0 & G^{-1}_{\mathrm{e}_1,k} & 0 & 0 \\ 0 & 0 & G^{-1}_{\mathrm{e}_2,k} & 0 \\ 0 & 0 & 0 & G^{-1}_{\mathrm{h}_2,k} \end{pmatrix} \;, \tag{A9}$$

$$\mathcal{V} = \begin{pmatrix} 0 & \mathbf{M}_{1,k-k'}\cdot\boldsymbol{\sigma} & \mathbf{M}_{2,k-k'}\cdot\boldsymbol{\sigma} & 0 \\ \mathbf{M}_{1,k-k'}\cdot\boldsymbol{\sigma} & 0 & 0 & \mathbf{M}_{2,k-k'}\cdot\boldsymbol{\sigma} \\ \mathbf{M}_{2,k-k'}\cdot\boldsymbol{\sigma} & 0 & 0 & \mathbf{M}_{1,k-k'}\cdot\boldsymbol{\sigma} \\ 0 & \mathbf{M}_{2,k-k'}\cdot\boldsymbol{\sigma} & \mathbf{M}_{1,k-k'}\cdot\boldsymbol{\sigma} & 0 \end{pmatrix} \;. \tag{A10}$$

We follow the usual route of integrating out the fermionic degrees of freedom in order to develop an effective theory in terms of the bosonic fields $\mathbf{M}_i$,

$$\begin{aligned} \frac{\mathcal{Z}}{\mathcal{Z}_0} &= \mathcal{Z}_0^{-1} \int \mathcal{D}\mathbf{M} \int \mathcal{D}[\bar{\psi},\psi]\, \mathrm{e}^{-\mathcal{S}[\mathbf{M},\bar{\psi},\psi]} = \int \mathcal{D}\mathbf{M} \mathrm{e}^{-\frac{1}{4V}\int_q (\mathbf{M}_{1,q}\cdot\mathbf{M}_{1,-q} + \mathbf{M}_{2,q}\cdot\mathbf{M}_{2,-q}) + \mathrm{tr}\ln(\mathbb{1}+\mathcal{G}_0\mathcal{V})} \\ &\simeq \mathrm{e}^{-\frac{1}{4V}(|\mathbf{M}_1|^2+|\mathbf{M}_2|^2)+\mathrm{tr}\ln(\mathbb{1}+\mathcal{G}_0\mathcal{V})} \equiv \mathrm{e}^{-\mathcal{S}_{\mathrm{MF}}[\mathbf{M}_1,\mathbf{M}_2]} \;, \end{aligned} \tag{A11}$$

where we employed a saddle-point approximation to the field integral in the second line in order to obtain the mean-field theory in terms of the fields $\mathbf{M}_i$ which we assume to be homogeneous and static here. As a final step, we can expand the logarithm according to $\mathrm{tr}\ln(\mathbb{1}+\mathcal{G}_0\mathcal{V}) \simeq -\frac{1}{2}(\mathcal{G}_0\mathcal{V})^2 - \frac{1}{4}(\mathcal{G}_0\mathcal{V})^4 + \ldots$ since the trace of odd powers of $\mathcal{G}_0\mathcal{V}$ vanishes. The resulting mean-field expression for the action up to quartic order in the order parameters $\mathbf{M}_1$ and $\mathbf{M}_2$ then reads

$$\mathcal{S}_{\mathrm{MF}}[\mathbf{M}_1,\mathbf{M}_2] = \sum_i a_i |\mathbf{M}_i|^2 + \sum_{i,j} u_{ij} |\mathbf{M}_i|^2 |\mathbf{M}_j|^2 + 2w(\mathbf{M}_1\cdot\mathbf{M}_2)^2 \;, \tag{A12}$$

and the corresponding coefficients are given by

$$a_i = \frac{1}{4V} + 2\int_k \left(G_{\mathrm{h}_1,k} G_{\mathrm{e}_i,k} + G_{\mathrm{h}_2,k} G_{\mathrm{e}_{\bar{i}},k}\right) \;, \tag{A13}$$

$$u_{ii} = \int_k \left(G^2_{\mathrm{h}_1,k} G^2_{\mathrm{e}_i,k} + G^2_{\mathrm{h}_2,k} G^2_{\mathrm{e}_{\bar{i}},k}\right) \;, \tag{A14}$$

$$u_{12} = u_{21} = \int_k \left[(G^2_{\mathrm{h}_1,k} + G^2_{\mathrm{h}_2,k}) G_{\mathrm{e}_1,k} G_{\mathrm{e}_2,k} + (G^2_{\mathrm{e}_1,k} + G^2_{\mathrm{e}_2,k}) G_{\mathrm{h}_1,k} G_{\mathrm{h}_2,k} - 2 G_{\mathrm{h}_1,k} G_{\mathrm{h}_2,k} G_{\mathrm{e}_1,k} G_{\mathrm{e}_2,k}\right] \;, \tag{A15}$$

$$w = 4\int_k G_{\mathrm{h}_1,k} G_{\mathrm{h}_2,k} G_{\mathrm{e}_1,k} G_{\mathrm{e}_2,k} \;, \tag{A16}$$

where we used $\mathrm{tr}(\sigma_i\sigma_j) = 2\delta_{ij}$ and $\mathrm{tr}(\sigma_i\sigma_j\sigma_k\sigma_l) = \delta_{ij}\delta_{kl} - \delta_{ik}\delta_{jl} + \delta_{il}\delta_{jk}$ for evaluating the traces in spin space. Upon neglecting the second hole pocket at the $M$ point, i. e. considering $E_M \to \infty$ implying $G_{\mathrm{h}_2,k} = 0$, we recover the results for the three-band model, as given in Eq. (8) and derived in Ref. 26, for instance.

The two electron bands are connected by rotational symmetry which translates to $\delta_m \leftrightarrow -\delta_m$ within the parametrization (3). This symmetry can be exploited to obtain the identities, $a_1 = a_2$ and $u_{11} = u_{22}$, which allow to further simplify the Ginzburg-Landau expansion. This can be seen most easily from expanding the propagators $G_{\mathrm{e}_i,k} = [\mathrm{i}\nu_n - \epsilon + \delta_\mu \mp \delta_m \cos(2\theta)]^{-1}$ for $\delta_m \ll 2\pi T$: The $n^{\mathrm{th}}$-order contribution is $\propto [\delta_m \cos(2\theta)]^n$. The electron propagators $G_{\mathrm{e}_1,k}$ and $G_{\mathrm{e}_2,k}$ therefore only differ in the odd terms which vanish upon performing the angular part of the momentum integration, $\int_0^{2\pi} \frac{\mathrm{d}\theta}{2\pi} \cos^{2n+1}(2\theta) = 0$.

## Appendix B: Calculation of the diagrams

This appendix provides technical details and intermediate steps of the calculation of the quartic coefficients of the Ginzburg-Landau expansion.

### 1. Clean four-band model

In the clean four-band model, i. e. including an incipient hole pocket at the $M$ point, the coefficient $w$ is already nonzero if all other pockets are nested, corresponding to $\delta_\mu = \delta_m = 0$,

$$\begin{aligned} w &= 4\int_k G_{\mathrm{h}_1,\mathbf{k}}(\nu_n)G_{\mathrm{h}_2,\mathbf{k}}(\nu_n)G_{\mathrm{e}_1,\mathbf{k}}(\nu_n)G_{\mathrm{e}_2,\mathbf{k}}(\nu_n) \\ &= 4T\sum_{n=-\infty}^{\infty}\int \frac{\mathrm{d}\mathbf{k}}{(2\pi)^2}\,\frac{1}{\mathrm{i}\nu_n+\epsilon_{\mathbf{k}}}\,\frac{1}{\mathrm{i}\nu_n+\epsilon_{\mathbf{k}}+E_M}\,\frac{1}{(\mathrm{i}\nu_n-\epsilon_{\mathbf{k}})^2} \\ &= 4T\sum_{n=-\infty}^{\infty}\rho_{\mathrm{F}}\int_{-\infty}^{\infty}\mathrm{d}\epsilon\,\frac{1}{\mathrm{i}\nu_n+\epsilon}\,\frac{1}{\mathrm{i}\nu_n+\epsilon+E_M}\,\frac{1}{(\mathrm{i}\nu_n-\epsilon)^2} \\ &= 4T\sum_{n=-\infty}^{\infty}\mathrm{sgn}(\omega_n)\frac{\mathrm{i}\pi\rho_{\mathrm{F}}E_M-4\pi\rho_{\mathrm{F}}\omega_n}{2\omega_n^2(E_M+2\mathrm{i}\omega_n)^2} \\ &= \frac{\mathrm{i}\rho_{\mathrm{F}}}{2E_M\pi T}\left[\psi_1\left(\frac{1}{2}+\frac{\mathrm{i}E_M}{4\pi T}\right)-\psi_1\left(\frac{1}{2}-\frac{\mathrm{i}E_M}{4\pi T}\right)\right] \\ &\approx \begin{cases} \frac{7\rho_{\mathrm{F}}\zeta(3)}{2\pi^2T^2}\approx 0.43\frac{\rho_{\mathrm{F}}}{T^2} & , \quad E_M \ll T\,, \\ \frac{4\rho_{\mathrm{F}}}{E_M^2} & , \quad E_M \gg T\,, \end{cases} \end{aligned} \tag{B1}$$

where $\rho_{\mathrm{F}}$ denotes the density of states at the Fermi surface and $\nu_n = \pi T(2n+1)$ is a fermionic Matsubara frequency.

### 2. Disordered three-band model

The diagrammatic representation of contributions to the quartic coefficients in the disordered three-band model, i. e. when neglected the incipient hole pocket at the $M$ point, is given in Fig. 4. The coefficients in terms of these diagrams read

$$g = \mathcal{G}_2^{(1)} - \mathcal{G}_1^{(1)} + \mathcal{G}_2^{(2)} - \mathcal{G}_1^{(2)}\,, \tag{B2}$$

$$u = \mathcal{G}_1^{(1)} + \mathcal{G}_2^{(1)} + \mathcal{G}_1^{(2)} + \mathcal{G}_2^{(2)}\,, \tag{B3}$$

$$w = 2\mathcal{W}\,. \tag{B4}$$

The corresponding expressions can be evaluated in the same manner as in the clean four-band model. However, since we now consider elliptical electron bands and finite detuning, we expand in the small parameters $\delta_\mu/(2\pi T)$ and $\delta_m/(2\pi T)$. Furthermore, we split the momentum integration according to $\int \frac{\mathrm{d}\mathbf{k}}{(2\pi)^2}\ldots = \rho_{\mathrm{F}}\int_{-\infty}^{\infty}\mathrm{d}\epsilon\int_0^{2\pi}\frac{\mathrm{d}\theta}{2\pi}\ldots$. Straightforward evaluation of the coefficients yields

$$\begin{aligned} g &= -\frac{T}{2}\sum_n\int\frac{\mathrm{d}\mathbf{k}}{(2\pi)^2}G_{\mathrm{h}_\Gamma,\mathbf{k}}^2(\nu_n)\left[G_{\mathrm{e}_1,\mathbf{k}}(\nu_n)-G_{\mathrm{e}_2,\mathbf{k}}(\nu_n)\right]^2 - \Gamma_{\mathrm{h}}^{\mathrm{intra}}\frac{T}{2}\sum_n\left[\int\frac{\mathrm{d}\mathbf{k}}{(2\pi)^2}G_{\mathrm{h}_\Gamma,\mathbf{k}}^2(\nu_n)[G_{\mathrm{e}_1,\mathbf{k}}(\nu_n)-G_{\mathrm{e}_2,\mathbf{k}}(\nu_n)]\right]^2 \\ &= -\frac{\rho_{\mathrm{F}}\delta_m^2}{1536\pi^4T^4}\left[\psi_4\left(\frac{1}{2}+\frac{\rho_{\mathrm{F}}\Gamma_{\mathrm{h}}^{\mathrm{intra}}}{4T}\right)-\frac{\delta_\mu^2}{32\pi^2T^2}\,\psi_6\left(\frac{1}{2}+\frac{\rho_{\mathrm{F}}\Gamma_{\mathrm{h}}^{\mathrm{intra}}}{4T}\right)\right] \end{aligned} \tag{B5}$$

$$\begin{aligned} u &= \frac{T}{2}\sum_n\int\frac{\mathrm{d}\mathbf{k}}{(2\pi)^2}\,G_{\mathrm{h}_\Gamma,\mathbf{k}}^2(\nu_n)\left[G_{\mathrm{e}_1,\mathbf{k}}(\nu_n)+G_{\mathrm{e}_2,\mathbf{k}}(\nu_n)\right]^2 + \Gamma_{\mathrm{h}}^{\mathrm{intra}}\frac{T}{2}\sum_n\left[\int\frac{\mathrm{d}\mathbf{k}}{(2\pi)^2}\,G_{\mathrm{h}_\Gamma,\mathbf{k}}^2(\nu_n)[G_{\mathrm{e}_1,\mathbf{k}}(\nu_n)+G_{\mathrm{e}_2,\mathbf{k}}(\nu_n)]\right]^2 \\ &= -\frac{\rho_{\mathrm{F}}}{8\pi^2T^2}\left[\psi_2\left(\frac{1}{2}+\frac{\rho_{\mathrm{F}}\Gamma_{\mathrm{h}}^{\mathrm{intra}}}{4T}\right)+\frac{\rho_{\mathrm{F}}\Gamma_{\mathrm{h}}^{\mathrm{intra}}}{12T}\,\psi_3\left(\frac{1}{2}+\frac{\rho_{\mathrm{F}}\Gamma_{\mathrm{h}}^{\mathrm{intra}}}{4T}\right)\right] \\ &\quad + \frac{\rho_{\mathrm{F}}}{768\pi^4T^4}\,\psi_4\left(\frac{1}{2}+\frac{\rho_{\mathrm{F}}\Gamma}{4T}\right)\left[3\delta_\mu^2+\delta_m^2\right] + \frac{\rho_{\mathrm{F}}^2\Gamma_{\mathrm{h}}^{\mathrm{intra}}}{30720\pi^4T^5}\,\psi_5\left(\frac{1}{2}+\frac{\rho_{\mathrm{F}}\Gamma}{4T}\right)\left[10\delta_\mu^2+3\delta_m^2\right] \end{aligned} \tag{B6}$$

$$\begin{aligned} w &= 2\Gamma_{\mathrm{e-e}}^{\mathrm{inter}}T\sum_n\left[\int\frac{\mathrm{d}\mathbf{k}}{(2\pi)^2}\,G_{\mathrm{h}_\Gamma,\mathbf{k}}(\nu_n)G_{\mathrm{e}_1,\mathbf{k}}(\nu_n)G_{\mathrm{e}_2,\mathbf{k}}(\nu_n)\right]^2 \\ &= -\frac{\rho_{\mathrm{F}}^2\Gamma_{\mathrm{e-e}}^{\mathrm{inter}}}{96\pi^2T^3}\left[\psi_3\left(\frac{1}{2}+\frac{\rho_{\mathrm{F}}(\Gamma_{\mathrm{h}}^{\mathrm{intra}}+\Gamma_{\mathrm{e-e}}^{\mathrm{inter}})}{4T}\right)-\frac{10\delta_\mu^2+\delta_m^2}{320\pi^2T^2}\,\psi_5\left(\frac{1}{2}+\frac{\rho_{\mathrm{F}}(\Gamma_{\mathrm{h}}^{\mathrm{intra}}+\Gamma_{\mathrm{e-e}}^{\mathrm{inter}})}{4T}\right)\right]\,. \end{aligned} \tag{B7}$$

[1] Johnpierre Paglione and Richard L. Greene, "High-temperature superconductivity in iron-based materials," Nature Physics **6**, 645–658 (2010).

[2] Andrey V. Chubukov and Peter J. Hirschfeld, "Fe-based superconductors: seven years later," Physics Today **68**, 46 (2015).

[3] D. K. Pratt, W. Tian, A. Kreyssig, J. L. Zarestky, S. Nandi, N. Ni, S. L. Bud'ko, P. C. Canfield, A. I. Goldman, and R. J. McQueeney, "Coexistence of competing antiferromagnetic and superconducting phases in the underdoped $Ba(Fe_{0.953}Co_{0.047})_2As_2$ compound using x-ray and neutron scattering techniques," Phys. Rev. Lett. **103**, 087001 (2009).

[4] Y. Laplace, J. Bobroff, F. Rullier-Albenque, D. Colson, and A. Forget, "Atomic coexistence of superconductivity and incommensurate magnetic order in the pnictide $Ba(Fe_{1-x}Co_x)_2As_2$," Phys. Rev. B **80**, 140501 (2009).

[5] Chen Fang, Hong Yao, Wei-Feng Tsai, JiangPing Hu, and Steven A. Kivelson, "Theory of electron nematic order in LaFeAsO," Phys. Rev. B **77**, 224509 (2008).

[6] Cenke Xu, Markus Müller, and Subir Sachdev, "Ising and spin orders in the iron-based superconductors," Phys. Rev. B **78**, 020501 (2008).

[7] R. M. Fernandes, A. V. Chubukov, and J. Schmalian, "What drives nematic order in iron-based superconductors?" Nat. Phys. **10**, 97–104 (2014).

[8] A. Jesche, C. Krellner, M. de Souza, M. Lang, and C. Geibel, "Coupling between the structural and magnetic transition in CeFeAsO," Phys. Rev. B **81**, 134525 (2010).

[9] Takasada Shibauchi, private communication.

[10] Shuhua Liang, Christopher B. Bishop, Adriana Moreo, and Elbio Dagotto, "Isotropic in-plane quenched disorder and dilution induce a robust nematic state in electron-doped pnictides," Phys. Rev. B **92**, 104512 (2015).

[11] M. G. Kim, A. Kreyssig, A. Thaler, D. K. Pratt, W. Tian, J. L. Zarestky, M. A. Green, S. L. Bud'ko, P. C. Canfield, R. J. McQueeney, and A. I. Goldman, "Antiferromagnetic ordering in the absence of structural distortion in $Ba(Fe_{1-x}Mn_x)_2As_2$," Phys. Rev. B **82**, 220503(R) (2010).

[12] Avci S., Chmaissem O., Allred J.M., Rosenkranz S., Eremin I., Chubukov A.V., Bugaris D.E., Chung D.Y., Kanatzidis M.G., Castellan J.-P, Schlueter J.A., Claus H., Khalyavin D.D., Manuel P., Daoud-Aladine A., and Osborn R., "Magnetically driven suppression of nematic order in an iron-based superconductor," Nat. Commun. **5**, 3845 (2014).

[13] L. Wang, F. Hardy, A. E. Böhmer, T. Wolf, P. Schweiss, and C. Meingast, "Complex phase diagram of $Ba_{1-x}Na_xFe_2As_2$: a multitude of phases striving for the electronic entropy," Phys. Rev. B **93**, 014514 (2016).

[14] E. Hassinger, G. Gredat, F. Valade, S. René de Cotret, A. Juneau-Fecteau, J.-Ph. Reid, H. Kim, M. A. Tanatar, R. Prozorov, B. Shen, H.-H. Wen, N. Doiron-Leyraud, and Louis Taillefer, "Pressure-induced Fermi-surface reconstruction in the iron-arsenide superconductor $Ba_{1-x}K_xFe_2As_2$: Evidence of a phase transition inside the antiferromagnetic phase," Phys. Rev. B **86**, 140502 (2012).

[15] Böhmer A. E., Hardy F., Wang L., Wolf T., Schweiss P., and Meingast C., "Superconductivity-induced re-entrance of the orthorhombic distortion in $Ba_{1-x}K_xFe_2As_2$," Nat. Commun. **6**, 7911 (2015).

[16] J. M. Allred, S. Avci, D. Y. Chung, H. Claus, D. D. Khalyavin, P. Manuel, K. M. Taddei, M. G. Kanatzidis, S. Rosenkranz, R. Osborn, and O. Chmaissem, "Tetragonal magnetic phase in $Ba_{1-x}K_xFe_2As_2$ from x-ray and neutron diffraction," Phys. Rev. B **92**, 094515 (2015).

[17] E. Hassinger, G. Gredat, F. Valade, S. Rene de Cotret, O. Cyr-Choiniere, A. Juneau-Fecteau, J.-Ph. Reid, M. H. Kim, A. Tanatar, R. Prozorov, B. Shen, H.-H. Wen, N. Doiron-Leyraud, and L. Taillefer, "Expansion of the tetragonal magnetic phase with pressure in the iron-arsenide superconductor $Ba_{1-x}K_xFe_2As_2$," arXiv:1512.05912 (2015).

[18] J. M. Allred, K. M. Taddei, D. E. Bugaris, M. J. Krogstad, S. H. Lapidus, D. Y. Chung, H. Claus, M. G. Kanatzidis, D. E. Brown, J. Kang, R. M. Fernandes, I. Eremin, S. Rosenkranz, O. Chmaissem, and R. Osborn, "Double-Q spin-density wave in iron arsenide superconductors," arXiv:1505.06175.

[19] Xiaoyu Wang, Jian Kang, and Rafael M. Fernandes, "Magnetic order without tetragonal-symmetry-breaking in iron arsenides: Microscopic mechanism and spin-wave spectrum," Phys. Rev. B **91**, 024401 (2015).

[20] R. M. Fernandes, S. A. Kivelson, and E. Berg, "Vestigial chiral and charge orders from bidirectional spin-density waves: Application to the iron-based superconductors," Phys. Rev. B **93**, 014511 (2016).

[21] J. Lorenzana, G. Seibold, C. Ortix, and M. Grilli, "Competing orders in FeAs layers," Phys. Rev. Lett. **101**, 186402 (2008).

[22] I. Eremin and A. V. Chubukov, "Magnetic degeneracy and hidden metallicity of the spin-density-wave state in ferropnictides," Phys. Rev. B **81**, 024511 (2010).

[23] Jian Kang and Zlatko Tešanović, "Theory of the valley-density wave and hidden order in iron pnictides," Phys. Rev. B **83**, 020505 (2011).

[24] Gianluca Giovannetti, Carmine Ortix, Martijn Marsman, Massimo Capone, Jeroen von den Brink, and José Lorenzana, "Proximity of iron pnictide superconductors to a quantum tricritical point," Nature Communications **2**, 398 (2011).

[25] P. M. R. Brydon, Jacob Schmiedt, and Carsten Timm, "Microscopically derived Ginzburg-Landau theory for magnetic order in the iron pnictides," Phys. Rev. B **84**, 214510 (2011).

[26] R. M. Fernandes, A. V. Chubukov, J. Knolle, I. Eremin, and J. Schmalian, "Preemptive nematic order, pseudogap, and orbital order in the iron pnictides," Phys. Rev. B **85**, 024534 (2012).

[27] Vladimir Cvetkovic and Oskar Vafek, "Space group symmetry, spin-orbit coupling, and the low-energy effective hamiltonian for iron-based superconductors," Phys. Rev. B **88**, 134510 (2013).

[28] Jian Kang, Xiaoyu Wang, Andrey V. Chubukov, and Rafael M. Fernandes, "Interplay between tetragonal magnetic order, stripe magnetism, and superconductivity in iron-based materials," Phys. Rev. B **91**, 121104 (2015).

[29] Maria N. Gastiasoro and Brian M. Andersen, "Competing magnetic double-$Q$ phases and superconductivity-induced reentrance of $C_2$ magnetic stripe order in iron pnictides," Phys. Rev. B **92**, 140506 (2015).

[30] Xiaoyu Wang and Rafael M. Fernandes, "Impact of local-moment fluctuations on the magnetic degeneracy of iron arsenide superconductors," Phys. Rev. B **89**, 144502 (2014).

[31] F. Waßer, A. Schneidewind, Y. Sidis, S. Wurmehl, S. Aswartham, B. Büchner, and M. Braden, "Spin reorientation in $Ba_{0.65}Na_{0.35}Fe_2As_2$ studied by single-crystal neutron diffraction," Phys. Rev. B **91**, 060505 (2015).

[32] B. P. P. Mallett, Yu. G. Pashkevich, A. Gusev, Th. Wolf, and C. Bernhard, "Muon spin rotation study of the magnetic structure in the tetragonal antiferromagnetic state of weakly underdoped $Ba_{1-x}K_xFe_2As_2$," Europhys. Lett. **111**, 57001 (2015).

[33] P. Chandra, P. Coleman, and A. I. Larkin, "Ising transition in frustrated Heisenberg models," Phys. Rev. Lett. **64**, 88–91 (1990).

[34] Morten H. Christensen, Jian Kang, Brian M. Andersen, Ilya Eremin, and Rafael M. Fernandes, "Spin reorientation driven by the interplay between spin-orbit coupling and Hund's rule coupling in iron pnictides," Phys. Rev. B **92**, 214509 (2015).

[35] Saurabh Maiti and Andrey V. Chubukov, "Renormalization group flow, competing phases, and the structure of superconducting gap in multiband models of iron-based superconductors," Phys. Rev. B **82**, 214515 (2010).

[36] R. M. Fernandes, M. G. Vavilov, and A. V. Chubukov, "Enhancement of $T_c$ by disorder in underdoped iron pnictide superconductors," Phys. Rev. B **85**, 140512 (2012).

[37] H. Wadati, I. Elfimov, and G. A. Sawatzky, "Where are the extra $d$ electrons in transition-metal-substituted iron pnictides?" Phys. Rev. Lett. **105**, 157004 (2010).

[38] M. Hoyer, M. S. Scheurer, S. V. Syzranov, and J. Schmalian, "Pair breaking due to orbital magnetism in iron-based superconductors," Phys. Rev. B **91**, 054501 (2015).

[39] A. E. Karkin, J. Werner, G. Behr, and B. N. Goshchitskii, "Neutron-irradiation effects in polycrystalline $LaFeAsO_{0.9}F_{0.1}$ superconductors," Phys. Rev. B **80**, 174512 (2009).

[40] Jun Li, Yanfeng Guo, Shoubao Zhang, Shan Yu, Yoshihiro Tsujimoto, Hiroshi Kontani, Kazunari Yamaura, and Eiji Takayama-Muromachi, "Linear decrease of critical temperature with increasing Zn substitution in the iron-based superconductor $BaFe_{1.89-2x}Zn_{2x}Co_{0.11}As_2$," Phys. Rev. B **84**, 020513 (2011).

[41] Kevin Kirshenbaum, S. R. Saha, S. Ziemak, T. Drye, and J. Paglione, "Universal pair-breaking in transition-metal-substituted iron-pnictide superconductors," Phys. Rev. B **86**, 140505 (2012).

[42] F. Rullier-Albenque, D. Colson, A. Forget, and H. Alloul, "Hall Effect and Resistivity Study of the Magnetic Transition, Carrier Content, and Fermi-Liquid Behavior in $Ba(Fe_{1-x}Co_x)_2As_2$," Phys. Rev. Lett. **103**, 057001 (2009).

[43] Lei Fang, Huiqian Luo, Peng Cheng, Zhaosheng Wang, Ying Jia, Gang Mu, Bing Shen, I. I. Mazin, Lei Shan, Cong Ren, and Hai-Hu Wen, "Roles of multiband effects and electron-hole asymmetry in the superconductivity and normal-state properties of $Ba(Fe_{1-x}Co_x)_2As_2$," Phys. Rev. B **80**, 140508 (2009).

[44] M. P. Allan, A. W. Rost, A. P. Mackenzie, Y. Xie, J. C. Davis, K. Kihou, C. H. Lee, A. Iyo, H. Eisaki, and T.-M. Chuang, "Anisotropic Energy Gaps of Iron-Based Superconductivity from Intraband Quasiparticle Interference in LiFeAs," Science **336**, 563–567 (2012).

[45] Tom Berlijn, Chia-Hui Lin, William Garber, and Wei Ku, "Do transition-metal substitutions dope carriers in iron-based superconductors?" Phys. Rev. Lett. **108**, 207003 (2012).

[46] Alexander Herbig, Rolf Heid, and Jörg Schmalian, "Charge doping versus impurity scattering in chemically substituted iron-pnictides," arXiv:1510.06941 (2015).

[47] Laura Fanfarillo, Alberto Cortijo, and Belén Valenzuela, "Spin-orbital interplay and topology in the nematic phase of iron pnictides," Phys. Rev. B **91**, 214515 (2015).

[48] Morten H. Christensen, Jian Kang, Brian M. Andersen, and Rafael M. Fernandes, "Spin-driven nematic instability of the multiorbital hubbard model: Application to iron-based superconductors," Phys. Rev. B **93**, 085136 (2016).

[49] M. Hoyer, S. V. Syzranov, and J. Schmalian, "Effect of weak disorder on the phase competition in iron pnictides," Phys. Rev. B **89**, 214504 (2014).

[50] Y. Wang, A. Kreisel, P. J. Hirschfeld, and V. Mishra, "Using controlled disorder to distinguish $s_{\pm}$ and $s_{++}$ gap structure in Fe-based superconductors," Phys. Rev. B **87**, 094504 (2013).